Eur. Phys. J. D **28**, 211–218 (2004)
DOI: 10.1140/epjd/e2003-00306-3

THE EUROPEAN PHYSICAL JOURNAL D

Excited states dynamics in time-dependent density functional theory

High-field molecular dissociation and harmonic generation

A. Castro[1,2,3,a], M.A.L. Marques[2,4,5], J.A. Alonso[1,2], G.F. Bertsch[3], and A. Rubio[2,5]

[1] Departamento de Física Teórica, Universidad de Valladolid, 47011 Valladolid, Spain
[2] Donostia International Physics Centre (DIPC), 20018 San Sebastián, Spain
[3] Physics Department and Institute for Nuclear Theory, University of Washington, Seattle WA 98195, USA
[4] Institut für Theoretische Physik, Freie Universität Berlin, 14175 Berlin, Germany
[5] Departamento de Física de Materiales and Centro Mixto CSIC-UPV/EHU, Facultad de Químicas, Universidad del País Vasco, 20018 San Sebastián, Spain

Received 22 January 2003 / Received in final form 15 October 2003
Published online 2nd December 2003 –

Abstract. We present numerical simulations of femtosecond laser induced dynamics of some selected simple molecules — hydrogen, singly ionized sodium dimer, singly ionized helium trimer and lithium cyanide. The simulations were performed within a real-space, real-time, implementation of time-dependent density functional theory (TDDFT). High harmonic generation, Coulomb explosion and laser induced photodissociation are observed. The scheme also describes non-adiabatic effects, such as the appearance of even harmonics for homopolar but isotopically asymmetric dimers, even if the ions are treated classically. This TDDFT-based method is reliable, scalable, and extensible to other phenomena such as photoisomerization, molecular transport and chemical reactivity.

PACS. 33.80.Gj Diffuse spectra; predissociation, photodissociation – 33.80.Wz Other multiphoton processes

1 Introduction

It is now possible to study electron and molecular dynamics in real time using various experimental techniques employing intense ultra-short laser sources [1]. Some examples of such investigations include X-ray photoelectron spectroscopy of molecules [2], pump-probe ionization measurements [3], production of high harmonics as a source of soft X-rays [4], the measurement of electron-phonon interactions in thin films [5], and the estimation of the onset of Coulomb screening [6]. A technologically important and very active field of research is the application of ultra-short laser pulses to induce, control and monitor chemical reactions [7–9]. Whenever the intensity of the laser field is comparable to the molecular electronic fields, perturbative expansions break down and new processes appear, which are not fully understood from a microscopical point of view. Some examples of these novel processes are bond softening, vibrational population trapping, molecular alignment and above threshold dissociation. A practical and accurate computational framework to describe excited-state electron-ion dynamics is therefore still needed.

Not surprisingly, the smallest systems have attracted particular attention from both experimentalists and theoreticians, as a bench-horse to improve our understanding of electron dynamics at the femtosecond scale [10,11]. However, the methods used in these calculations cannot be easily extended to larger and more realistic systems. The exact quantum mechanical solution of a 3D system of more than three particles is certainly not feasible with state-of-the-art computers. 1-D models are much easier to handle, but they can not really be used as predictive tools for problems involving the interaction of lasers with large clusters or solid-state systems of technological relevance.

To tackle such a problem, time-dependent density functional theory (TDDFT) [17] appears as a valuable tool. Even with the simplest approximation to the exchange-correlation potential, the adiabatic local density approximation (ALDA), one obtains a very good compromise between computational ease and accuracy [18]. TDDFT can certainly be applied to large systems in non perturbative regimes, while providing a consistent treatment of electron correlation. It has been well tested in the study of electron excitations, like the optical absorption spectra in the linear regime [19,20]. Although almost all applications of TDDFT in the field of laser physics

[a] e-mail: alberto.castro@tddft.org

have only involved electronic dynamics, recent attempts have also been made at describing the coupled nuclear and electronic motion in laser fields [21], accounting for the nuclear motion classically. A full quantum mechanical treatment of the system could in principle be done within a multi-component TDDFT, although it has not been tried for more than three particles [22]. However, since many vibrational quanta are coherently excited, there is good motivation for the classical treatment of the nuclei. The purpose of this work is to illustrate a general method to study the coupled electronic and ionic dynamics of many-electron systems subject to strong laser fields. It is based on the quantum mechanical propagation of the electronic wave packet — described exactly within TDDFT — in time and space, combined with the classical motion of the nuclei. As the laser field populates the excited Born-Oppenheimer surfaces, this scheme includes diabatic effects in a natural way, while maintaining a good scaling with the size of the system. As an illustration we focused on: one and two electron dimers, namely Na_2^+ and the hydrogen molecule; and the trimers He_3^+ and lithium cyanide (LiCN/LiNC).

2 Methodology

The equations of motion for the electrons and the nuclei may be derived from the Lagrangian:

$$\mathcal{L} = \sum_\alpha \left[\frac{1}{2} m_\alpha \dot{\boldsymbol{R}}_\alpha^2 + Z_\alpha \boldsymbol{R}_\alpha \boldsymbol{\mathcal{E}}(t)\right] - \sum_{\alpha<\alpha'} \frac{Z_\alpha Z_{\alpha'}}{|\boldsymbol{R}_\alpha - \boldsymbol{R}_{\alpha'}|} + \sum_i \left\langle \phi_i \left| i\,\hbar \frac{\partial}{\partial t} - e\boldsymbol{x}\boldsymbol{\mathcal{E}}(t) \right| \phi_i \right\rangle - E_{\mathrm{DFT}}(\{\phi\},\{\boldsymbol{R}\}), \quad (1)$$

where m_α and Z_α are the nuclear mass and charge, respectively, E_{DFT} is the usual Kohn-Sham density functional, depending on the electron orbitals $\{\phi\}$ and the nuclear coordinates $\{\boldsymbol{R}\}$, and $\boldsymbol{\mathcal{E}}(t)$ is the time-dependent electric field from the laser pulse. Variation of the Lagrangian then yields Newton's equations for the nuclear coordinates,

$$m_\alpha \frac{\mathrm{d}^2 \boldsymbol{R}_\alpha}{\mathrm{d}t^2} = -\boldsymbol{\nabla}_{R_\alpha} E_{\mathrm{DFT}} - \sum_{\alpha'} \frac{(\boldsymbol{R}_\alpha - \boldsymbol{R}_{\alpha'}) Z_\alpha Z_{\alpha'}}{|\boldsymbol{R}_\alpha - \boldsymbol{R}_{\alpha'}|^3} + Z_\alpha\, \boldsymbol{\mathcal{E}}(t), \quad (2)$$

and the usual TDDFT equations for the orbital variables [17]. We solved these equations in real time, following the method of Yabana and Bertsch [19], using a real-space grid representation of the orbitals [23]. This scheme has the advantage that the Kohn-Sham Hamiltonian, H_{KS}, is a very sparse matrix. The forces in equation (2) are calculated with the help of a generalized Hellmann-Feynman theorem,

$$-\boldsymbol{\nabla}_{\boldsymbol{R}_\alpha} E_{\mathrm{DFT}} = -\sum_i \langle \phi_i | \boldsymbol{\nabla}_\alpha H_{\mathrm{KS}} | \phi_i \rangle. \quad (3)$$

For numerical reasons we represent the electron-ion interaction by norm-conserving non-local Troullier-Martins pseudopotentials [24]. All calculations have been done with our home-grown implementation of TDDFT, the octopus code; more details about the calculations may be obtained from [25].

3 Results

We have studied two different classes of highly non linear time-dependent problems: photofragmentation of dimers (the singly ionized sodium dimer) and trimers (the homonuclear He_3^+ and the heteronuclear lithium cyanide); and high harmonic generation by the hydrogen molecule.

3.1 Na_2^+

We now discuss the first case, the Na_2^+ dimer in a femtosecond laser field. It is a good test, since it has been exhaustively studied using a diverseness of approaches [8,13,26]. In particular, a recent experiment [8] focused on the photofragmentation of Na_2^+ in intense femtosecond laser fields. Using a pump-probe technique, the authors discovered that Na_2^+ dissociated in four different channels, ranging from simple field ionization followed by Coulomb explosion, to photodissociation on light-induced potentials, upon absorption of one, two or three photons. For these calculations, we used a uniform grid spacing of 0.3 Å, and the system was confined to a sphere of radius 10 Å. Within the pseudopotential approach used here, and neglecting core-valence exchange correlation effects, this problem reduces to a one-electron calculation that can be solved exactly without any further approximations. In this case the total electronic energy is given by the Kohn-Sham eigenvalues, and they can be used to compute the adiabatic potential energy surfaces shown in Figure 1. The two lowest single-photon transitions from the $1^2\Sigma_g^+$ ground state are at 2.5 eV (to the $1^2\Sigma_u^+$ state) and at 3.2 eV (to the $1^2\Pi_u$ state). The latter is achieved by a laser polarized perpendicularly to the internuclear axis. These energies accord well with the observed single-photon transitions [27]. For the time-dependent calculations, we start with the dimer in its ground state. The ground state Kohn-Sham wavefunctions are then propagated with a unitary scheme [25]. The time step for the time integration was $0.005\ \hbar\ \mathrm{eV}^{-1} \approx 0.003$ fs. A simple check on the implementation of the time evolution operator consists of calculating the linear photo-absorption spectrum, using a weak δ-function external field, as in reference [19]. Almost all the spectral weight is concentrated in two peaks (see inset in Fig. 1), which are at energies corresponding exactly to the vertical transitions between the energy surfaces. We note that this exact correspondence is only obtained for one-electron systems: in general the TDDFT spectra does not coincide with the differences between Kohn-Sham eigenvalues, due to many-body effects.

Next we examine the evolution of the dimer under high-field excitation. We consider external fields of the

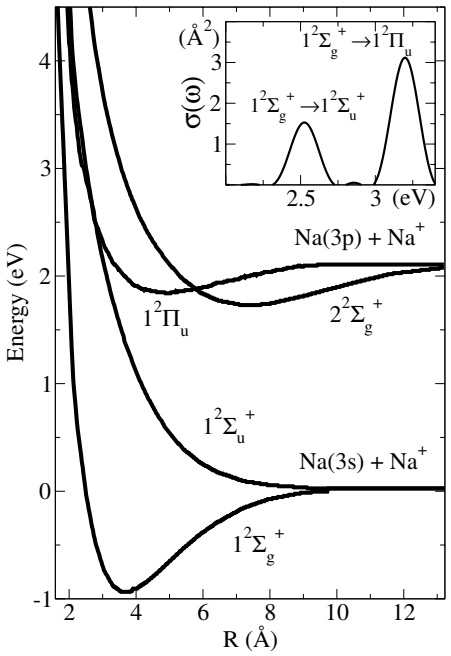

Fig. 1. Adiabatic energy surfaces of the Na_2^+ dimer, as obtained by our three-dimensional real-space code. Similar results can be found in reference [32]. In the inset, the computed photoabsorption cross-section of the same molecule.

form:

$$\boldsymbol{\mathcal{E}}(t) = \left(\frac{8\pi}{c} I_0\right)^{1/2} \sin\left(\pi \, \frac{t}{\tau}\right) \sin(\omega t)\hat{\boldsymbol{e}}, \quad 0 < t < \tau, \quad (4)$$

where I_0 is the maximum intensity of the pulse, $\hat{\boldsymbol{e}}$ is the polarization vector, and $\tau = 80\,\text{fs}$ is the pulse duration. As a first case, we examine the effect of excitation at the lower resonant frequency, $\omega = 2.5$ eV. In Figure 2a, we present a series of runs at different intensities, ranging from weak (10^{10} W/cm^2) to moderate (2.1×10^{12} W/cm^2). Since the $1^2\Sigma_u^+$ surface is anti-bonding, excitation at this resonant frequency should lead to dissociation, even at moderate intensities. This is indeed confirmed by our calculations. The upper panel depicts the internuclear separation of the dimer, which exhibits an acceleration during the laser pulse and a nearly constant velocity expansion thereafter. Clearly, the dimer dissociates at all field intensities that we applied. To examine the ionization of the dimer, we assumed that any density reaching the edges of the simulation box corresponds to unbound electrons. We then define the ionization probability as $I(t) = 1 - N(t)$, where $N(t)$ is the charge that remains inside the simulation box at time t. Note that ionization, defined in this way, also includes spurious contributions from bound electrons. This problem can be minimized by enlarging the size of the box. The lower panel of Figure 2a shows N as a function of t. We see that there is practically no ionization for the lower fields, and only a 20% ionization probability for the 2.1×10^{12} W/cm^2 field. Thus, in this range of intensities, the laser dissociates the dimer without ionizing it.

We next consider the excitation at the upper resonance frequency, $\omega = 3.2\,\text{eV}$, corresponding to an electric field perpendicular to the dimer axis [see Fig. 2b]. Since the $1^2\Pi_u$ surface is bonding, no dissociation is expected unless the Coulomb explosion channel is opened through ionization. We see that the dimer remains bound over the entire range of intensities that produced dissociation at the lower resonant frequency.

Finally, we also performed simulations at the non-resonant frequency $\omega = 1.57\,\text{eV}$, the one used in reference [8]. Figure 2c shows how dissociation now occurs only at much higher intensities, and it is mainly due to ionization (which is almost absent in the resonant calculations for the range of intensities used): since Na_2^{2+} has no bound states, ionization is followed by immediate dissociation.

3.2 He_3^+

The singly ionized helium trimer is a more challenging problem, since it already contains five electrons and three nuclei. Systems containing helium are also difficult cases for our numerical treatment, since the pseudopotential of He is very steep — a grid spacing of 0.18 Å was necessary to obtain converged results. We have performed simulations on He_3^+, motivated by several reasons: (i) the system has been well studied previously: the geometry has been accurately predicted to be that of a linear symmetric trimer [28] by ab initio methods. Its optical spectroscopy has also been characterized both experimentally [29] and theoretically [30]. (ii) Haberland et al. [31] have performed experiments on the photodissociation of ionized rare gas trimers — including He_3^+ —, induced by a 10 ns laser pulse, with photon energies ranging from 1.5 to 6 eV. They utilized time-of-flight mass spectroscopy to observe the fragments. Their results support the picture of a linear trimer photo-excited to a totally repulsive state, coupled to the ground-state through a parallel transition moment: the two lateral atoms are expelled at high opposed velocity, whereas the central atom only gains a small velocity at either side. The positive charge generally localizes on one of the fast outer particles; (iii) the system is conceptually simple, easing interpretation: in Figure 3 the relevant potential energy curves are depicted. TDLDA calculations of the optical response have been performed varying the nuclear geometry along the given coordinate. The inset of the figure shows the result for the equilibrium geometry. It is clear that only one excited potential energy surface is of interest; the only relevant optical transition is the $\Sigma_g \to \Sigma_u$ at 5.0 eV. The experiments position this peak at ≈ 5.3 eV. This excited PES is totally repulsive, and as such photoinduced population of this state should lead to dissociation. (iv) we wanted to ascertain whether the simplest functionals (e.g. the LDA) could yield reasonable qualitative results for non-linear phenomena, even for a specially challenging problem such as a helium compound; (v) ionized rare gas trimers are interesting by themselves by their possible influence in excimer lasers efficiency.

We have performed a number of simulations using various sets of laser parameters, amongst whose the four samples shown in Figure 4. The shape of the laser pulse was

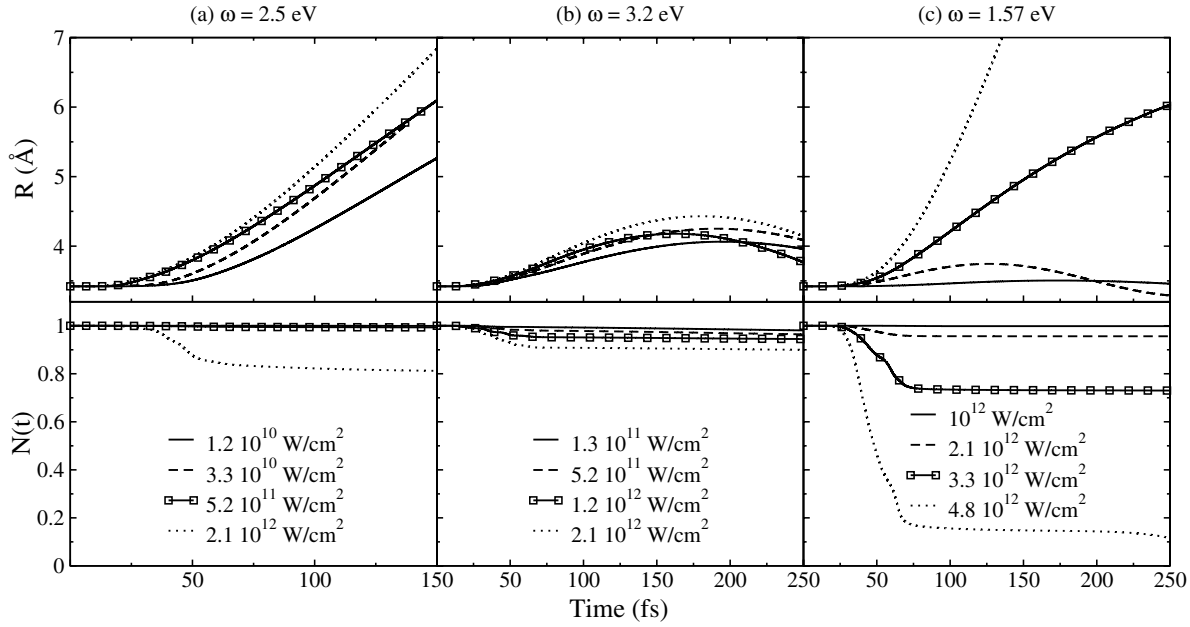

Fig. 2. Evolution of internuclear distance (top panel) and electronic charge in the simulation box (bottom panel) for the Na_2^+ molecule. The dimers are excited with laser pulses with photons of energy 2.5, 3.2 and 1.57 eV in columns (a), (b) and (c) respectively.

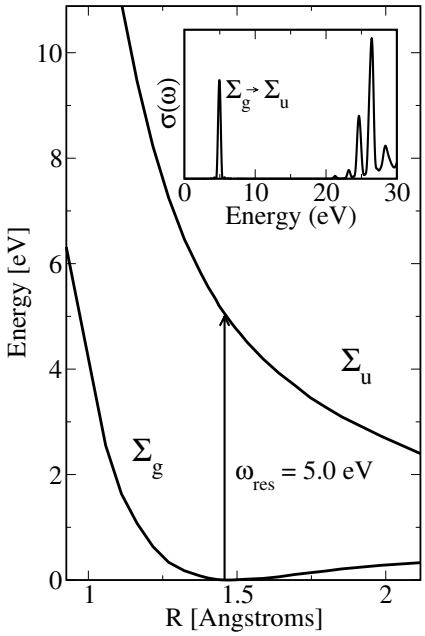

Fig. 3. Σ_g (ground state) and Σ_u potential energy surfaces. The abscissa corresponds to the simultaneous and symmetric displacement of the two outer atoms along the trimer axis. Inset: photoabsorption cross-section at equilibrium geometry. Calculations done at the TDLDA level.

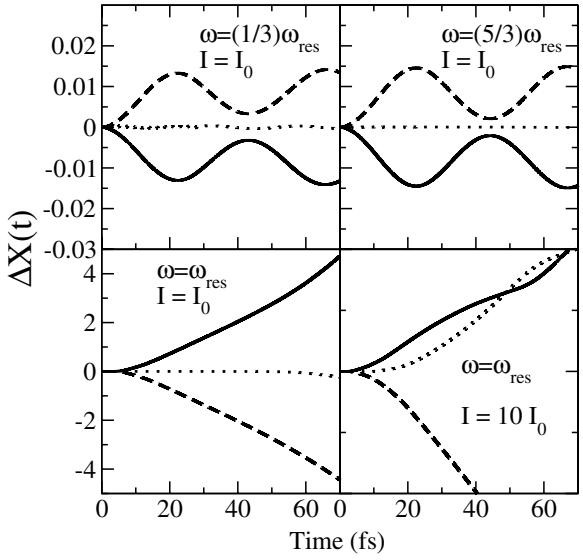

Fig. 4. Time-evolution of the three nuclear displacements (solid: top atom; dots: central atom; dashed: bottom atom) with respect to their original positions, along the trimer axis, for the frequencies and intensities given (ω_{res} = 5 eV, $I_0 = 8.8 \times 10^{11}$ W/cm^2).

identically trapezoidal in all four cases: an ascending linear ramp from 0 to ≈2.5 fs, a plateau of 25 fs, and then a descending linear ramp again of ≈2.5 fs. Intensities and frequencies, on the contrary, are different: top panels depict non-resonant cases, at one third (left) and five thirds (right) of the resonance $\Sigma_g \rightarrow \Sigma_u$ (5 eV). In both cases the two outer atoms only oscillate slightly around the equilibrium positions. Bottom panels are both resonant cases, with varying intensities. Two different dissociative channels are observed: in the left panel, a low intensity is provided, and the picture corresponds with the findings of Haberland et al. [31] — the two outer atoms gain high opposing velocities, whereas the central one remains almost unperturbed. Note that the intensity is the same as

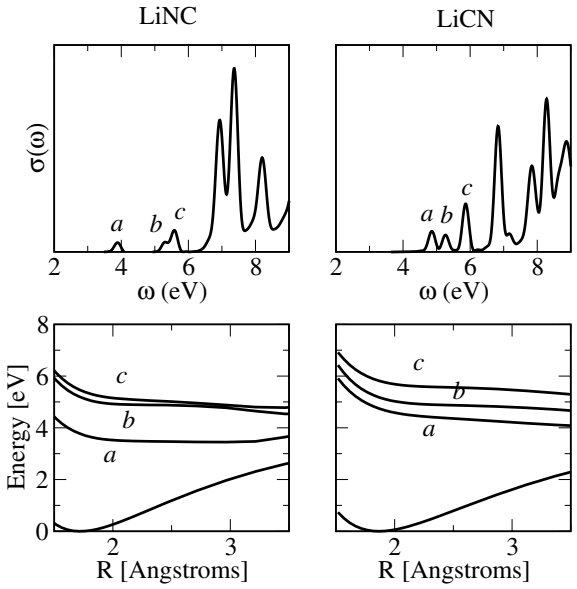

Fig. 5. Photoabsorption cross-section (in arbitrary units) of the LiCN and LiNC system at equilibrium geometries (top panels). PES of the lowest lying excited states, a, b and c, along the configuration space coordinate given by the elongation of the Li:CN bond (bottom panels).

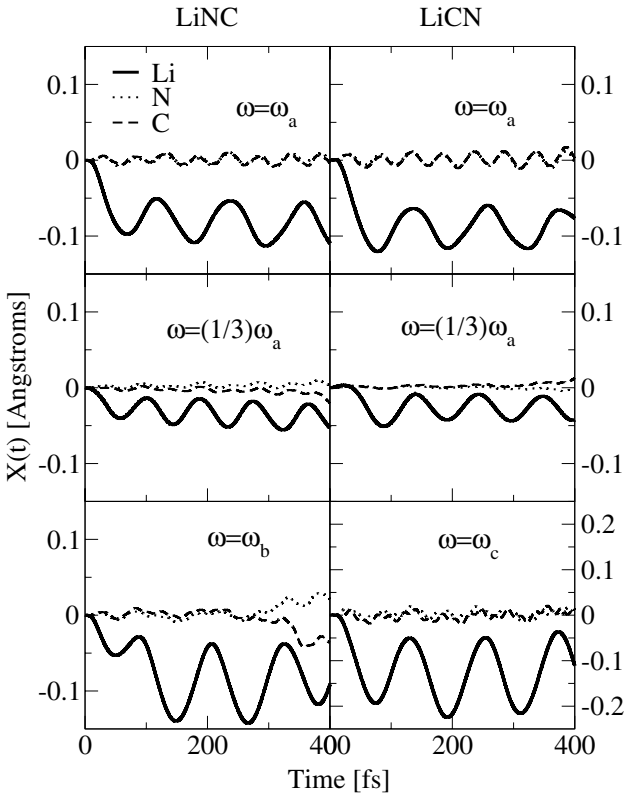

Fig. 6. Time-evolution of the coordinate of the atoms in the lithium cyanide system (for both LiNC — left — and LiCN — right — conformations) along the trimer axis. In each case, a laser pulse of identical length (100 fs) and intensity (1.3×10^{13} W/cm^2) was used, but different frequency, as marked in the graph. All coordinates are referred to their original position; since the initial lithium coordinate is negative, the negative displacements shown imply enlargement of distances from the lithium atom to the cyanide group.

the one used in the upper panels, where no dissociation was obtained. A higher intensity was used for the simulation shown in the bottom-right panel, and in this case the trimer dissociates into a dimer and an isolated atom. Most likely, the intensity of the nanosecond laser pulse used in the experiment is low, which agrees with the symmetric dissociative picture of the bottom-left panel.

3.3 Lithium cyanide (LiCN/LiNC)

We also tested the methodology with a heteronuclear trimer, the lithium cyanide molecule. This system has also been extensively studied theoretically [33], but no experimental results are available; our interest was attracted by the characteristics of the system: it consists of the floppy bonding of the cyanide group, CN (a well-known species of organic chemistry), to the light-weight, alkaline, lithium atom. It has two stable isomers, both of them linear, LiCN and LiNC. The typical chemistry picture of CN, which places most of the negative charge onto the C atom, would predict LiCN as the most stable isomer. Surprisingly, the LiNC structure is slightly lower in energy, yet very close to LiCN. The CN group is tightly bound together, whereas the lithium atom floats around it — the LiCN $\Leftrightarrow$ LiNC isomerization barrier is also small, ≈ 0.4 eV [34]. As a consequence, we may expect an easy photo-detachment of lithium from the CN group, which should remain bound.

The first step, as before, is the calculation of the excitation energies via TDDFT in the linear response regime. For this case, we have employed the generalized gradient approximation (GGA). Figure 5 shows the results. In the upper panels, the photoabsorption cross-section of both isomers was calculated at equilibrium distances. We will focus our attention to the lowest lying excitations, a, b and c. In the lower panels, the PES of these states is depicted. Two features are noteworthy: the little oscillation strength of those transitions, and the small dissociative slope of the energy curves, as compared to previous examples.

Our simulations are displayed in Figures 6 and 7. In Figure 6, the laser shape is trapezoidal: it is turned on at $t = 0$, ramps linearly to peak intensity (1.3×10^{13} W/cm^2) in a few femtoseconds, stays at peak intensity for about 100 fs, and then decays again linearly to zero. The two conformations, LiNC (left panels) and LiCN (right panels) have been studied. The frequencies have been tuned to: resonant to the first excitation, ω_a, in upper panels (3.89 eV for LiNC and 4.86 eV for LiCN); one third of these frequencies in middle panels; and resonant to the second ($\omega_b = 5.30$ eV) and third ($\omega_c = 5.87$ eV) excitation for LiNC and LiCN respectively, in the lower panels. Our objective was to study excitations to the higher-lying Born-Oppenheimer surfaces of the neutral system. Therefore we have chosen the highest possible intensity that,

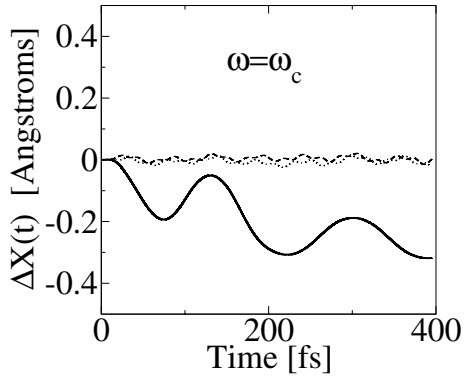

Fig. 7. Time-evolution of the coordinate of the atoms in the lithium cyanide system (for the LiCN conformation) along the trimer axis. In this case, the laser pulse ramps in about 10 fs to peak intensity (1.3×10^{13} W/cm^2) and then stays continuously for the whole simulation. The frequency is resonant to the third excitation.

for all six simulations, did not lead to ionization. The time lengths for these cases are much larger than for the Na_2^+ or He_3^+ systems, reaching almost half a picosecond. None of these cases, however, shows clear dissociative behavior. Due to the small oscillator strengths of these transitions, the systems did not absorb enough energy to populate significantly the excited energy surfaces. Moreover, as the slope of the excited energy surface is small, the molecule would take a very long time to dissociate.

We have tried to obtain dissociation by enlarging the time of exposure to the laser field, as shown if Figure 7 for LiCN. The laser was maintained at the peak intensity for the whole time window. In this case, there are much stronger evidences of dissociation. The ground state component, however, pulls back the lithium atom, so that in its trajectory a vibrational movement is superimposed to the main dissociative trend. However, by the end of the 400 fs, roughly one electron has been ionized. This is an artifact of the adiabatic GGA used in these calculations. As the GGA exchange and correlation (xc) potential, like the LDA and the meta-GGAs, has the wrong asymptotic behavior, it leads to too small ionization potentials. This result implies that for a proper description of the dissociation of this system, better xc functionals are needed, with the proper asymptotic behavior, to prevent ionization [35].

From these calculations, it is possible to extract information about the vibrational modes excited by the laser. As expected, the amplitudes of the nuclear vibrations for the resonant cases are much larger, since the energy absorption is more efficient. Quantitative information about the frequencies and intensities of the vibrational modes could be obtained from these simulations from the velocity autocorrelation function. However, for this purpose longer simulations times are needed, to obtain properly resolved spectra. This study, which in principle should allow to investigate resonant Raman spectra, is beyond the scope of this work, and will be addressed in a future publication.

3.4 High harmonic generation

Another process in which the nuclear motion might play an important role is high harmonic generation. Even harmonics may be created by irradiating HD with an intense laser pulse, but not by irradiating H_2: even harmonic generation is forbidden for a centrosymmetric molecule. In an adiabatic treatment of the nuclear coordinates, the nuclear masses play no role and the even harmonics can not appear. This is no longer the case if non-adiabatic effects are taken into account, for the different masses of H and D break the symmetry. Kreibich et al. [16] studied this process in a 1-D model with a full quantum mechanical treatment of the nuclear motion, finding strong even harmonics at high harmonic number. To discern whether the classical treatment of nuclear motion also produces these harmonics, we studied the same 1-D problem within our framework, using in this case the exact-exchange approximation to the exchange-correlation potential [36]. As in reference [16], we took the laser field to have a frequency of 1.6 eV, and an intensity that rises linearly to 10^{14} W/cm^2 over an interval of 10 optical cycles, and is held constant thereafter. We then calculated the spectral intensity of the generated harmonics, $H(\omega)$:

$$H(\omega) \sim \left| \int \mathrm{d}t \, e^{i\omega t} \, \frac{\mathrm{d}^2}{\mathrm{d}t^2} \left\langle \Psi(t) \right| \hat{\boldsymbol{e}} \cdot \boldsymbol{D} \left| \Psi(t) \right\rangle \right|^2 . \qquad (5)$$

We find that the classical treatment does indeed produce even harmonics, but much smaller than the quantum treatment. The results are shown in Figure 8. The top left panel depicts the harmonic spectrum for HD, and only odd harmonics are apparent. However, it may be proved that the HD Hamiltonian already violates centrosymmetry within our classical treatment, through a term of the form:

$$-\frac{1}{2}\left(\frac{1}{M_H} - \frac{1}{M_D}\right) P(t) \left(\hat{p}_1 + \hat{p}_2\right),$$

where $P(t) = \frac{1}{2}\left(P_H(t) - P_D(t)\right)$ is the relative time-dependent nuclear momentum and $\hat{p}_i$ are the electronic momentum operators [37]. Its effect can be enhanced by decreasing the nuclear masses. In the bottom left panel, the H and D masses have been decreased by a factor 100, and then the second- and fourth-order harmonics become visible. As a qualitative check of the numerics, we also show the same graphs for H_2, in which no even harmonics can occur.

Thus we see that on qualitative level the non-adiabatic dynamics generating even harmonics are obtained with the classical treatment of the nuclear coordinates. However, the quantum treatment may be needed for a quantitative result. By describing the nuclei quantum mechanically, the ground state violates centrosymmetry and the even harmonics can be generated. In contrast, in the classical treatment the electronic ground state is symmetric and the symmetry violation only builds up as the nuclei move.

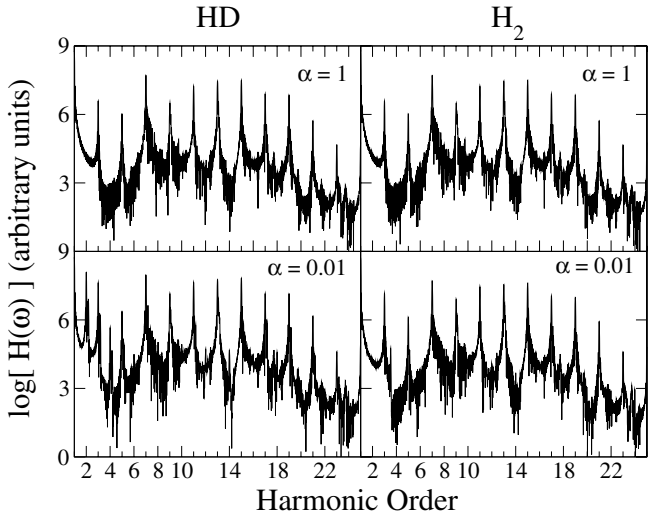

Fig. 8. Harmonic spectra of HD (left panels) and H_2 (right panels). The nuclear masses used in the calculation are $m' = \alpha m$, being m the real mass. In this way, top plots were made using for the nuclear masses their real values whereas bottom plots were made using a hundredth of their real values.

4 Conclusions

In summary, we have examined the computational feasibility of including nuclear dynamics in time-dependent density functional theory. Using this approach for some selected small molecules, we were able to distinguish different phodissociation regimes, ranging from dissociation on light induced potentials, to field ionization followed by Coulomb explosion. Electronic and ionic degrees of freedom are thus coupled, so that one can observe the electron-phonon transfer of energy. We also found, with another example, that non-adiabatic effects are present in the general treatment based on equation (1). One of the major attractivenesses of this method resides in its reasonable scaling behaviour when applied to larger systems. We thus expect to be able to tackle problems like photoisomerization or even photochemical reactivity in systems of dozens of atoms — without imposing any restriction in the description of the geometry — in the near future.

This work was supported by the European Community Research Training Networks NANOPHASE (HPRN-CT-2000-00167) and COMELCAN (HPRN-CT-2000-00128), by the Spanish MCyT (MAT2001-0946 and MAT2002-04499), by the University of the Basque Country (9/UPV 00206.215-13639/2001). The computer time was granted by CEPBA (Barcelona) and DIPC. GB acknowledges support by the US Department of Energy under Contract No. E-FG-06-90ER-411132. AC thanks the University of Washington and the DIPC for hospitality. JAA also thanks the DIPC for hospitality and support. We thank E.K.U. Gross for stimulating discussions.

References

1. For a review, see T. Brabec, F. Krausz, Rev. Mod. Phys. **72**, 545 (2000). For recent developments, see M. Drescher, M. Hentschel, R. Kienberger, G. Tempea, C. Spielmann, G.A. Reider, P.B. Corkum, F. Krausz, Science **291**, 1923 (2001); M. Hentschel, R. Kienberger, Ch. Spielmann, G.A. Reider, N. Milosevic, T. Brabec, P. Corkum, U. Heinzmann, M. Drescher, F. Krausz, Nature **414**, 509 (2001)
2. L.N. Glandorf, M. Scheer, M. Krishnamurthy, J.W. Odom, S.R. Leone, Phys. Rev. A **62**, 023812 (2000); L.N. Glandorf, M. Scheer, D.A. Samuels, A.M. Mulhisen, E.R. Grant, X. Yang, V.M. Bierbaum, S.R. Leone, Phys. Rev. Lett. **87**, 193002 (2001)
3. See, for example, articles in Faraday Discuss. **115** (2000)
4. Z. Chang, A. Rundquist, H. Wang, M.M. Murnane, H.C. Kapteyn, Phys. Rev. Lett. **79**, 2967 (1997); Ch. Spielmann, N.H. Burnett, S. Sartania, R. Koppitsch, M. Schnürer, C. Kan, M. Lenzner, P. Wobrauschek, F. Krausz, Science **278**, 661 (1997)
5. M. Probst, R. Haight, Appl. Phys. Lett. **71**, 202 (1997)
6. R. Huber, F. Tauser, A. Brodschelm, M. Bichler, G. Abstreiter, A. Leitenstorfer, Nature **414**, 286 (2001)
7. C.M. Dion, S. Chelkowski, A.D. Bandrauk, H. Humeda, Y. Fujimura, J. Chem. Phys. **105**, 9083 (1996); R.W. Shoenlein, L.A. Peteanu, R.A. Mathies, C.V. Shank, Science **254**, 412 (1991)
8. A. Assion, T. Baumert, U. Weichmann, G. Gerber, Phys. Rev. Lett. **86**, 5695 (2001)
9. K. Yamanouchi, Science **295**, 1659 (2002)
10. M. Protopapas, C.H. Keitel, P.L. Knight, Rep. Prog. Phys. **60**, 389 (1997)
11. Some of the works include exact 3D calculations for one and two electron atoms [12], for one electron dimers [13], and 1-D models for two electron systems [14–16]
12. J. Parker, K.T. Taylor, C.W. Clark, S. Blodgett-Ford, J. Phys. B **29**, L33 (1996)
13. S. Magnier, M. Persico, N. Rahman, J. Phys. Chem. A **103**, 10691 (1999)
14. R. Grobe, J.H. Eberly, Phys. Rev. A **48**, 4664 (1993); D.G. Lappas, A. Sanpera, J.B. Watson, K. Burnett, P.L. Knight, R. Grobe, J.H. Eberly, J. Phys. B **29**, L619 (1996)
15. M. Lein, E.K.U. Gross, V. Engel, Phys. Rev. A **64**, 023406 (2001)
16. T. Kreibich, M. Lein, V. Engel, E.K.U. Gross, Phys. Rev. Lett. **87**, 103901 (2001)
17. E. Runge, E.K.U. Gross, Phys. Rev. Lett. **52**, 997 (1984); E.K.U. Gross, J.F. Dobson, M. Petersilka, in *Density Functional Theory II*, edited by R.F. Nalewajski (Springer, Berlin, 1996); M.A.L. Marques, E.K.U. Gross, in *A Primer in Density Functional Theory*, edited by C. Fiolhais, F. Nogueira, M.A.L. Marques (Springer, Berlin, 2003)
18. The ALDA has some well known problems, but most of them can be solved by the swarm of exchange-correlation potential now available — see, for example, M.A.L. Marques, A. Castro, A. Rubio, J. Chem. Phys. **115**, 3006 (2001), and references therein
19. K. Yabana, G.F. Bertsch, Phys. Rev. B **54**, 4484 (1996); Int. J. Quant. Chem. **75**, 55 (1999)
20. G. Onida, L. Reining, A. Rubio, Rev. Mod. Phys. **74**, 601 (2002) and references therein
21. F. Calvayrac, P.-G. Reinhard, E. Suraud, C.A. Ullrich, Phys. Rep. **337**, 493 (2000); E. Suraud, P.G. Reinhard, Phys. Rev. Lett. **85**, 2296 (2000)

22. T. Kreibich, E.K.U. Gross, Phys. Rev. Lett. **86**, 2984 (2001)
23. J.R. Chelikowsky, N. Trouiller, Y. Saad, Phys. Rev. Lett. **72**, 1240 (1994); A. Rubio, J.A. Alonso, X. Blase, L.C. Balbás, S.G. Louie, Phys. Rev. Lett. **77**, 247 (1996); T.L. Beck, Rev. Mod. Phys. **72**, 1041 (2000)
24. N. Troullier, J.L. Martins, Phys. Rev. B **43**, 1993 (1991)
25. M.A.L. Marques, A. Castro, G.F. Bertsch, A. Rubio, Comp. Phys. Comm. **151**, 60 (2003). More information on `http://www.tddft.org/programs/octopus/`
26. S. Magnier, M. Persico, N. Rahman, Chem. Phys. Lett. **262**, 747 (1996); M. Machholm, A. Suzor-Weiner, J. Chem. Phys. **105**, 971 (1996)
27. V. Bonačić-Koutecký, J. Pittner, C. Fuchs, P. Fantucci, M.F. Guest, J. Koutecký, J. Chem. Phys. **104**, 1427 (1996)
28. M. Rosi, C.W. Bauschlicher Jr, Chem. Phys. Lett. **159**, 479 (1989); V. Staemmler, Z. Phys. D **22**, 741 (1992); F.X. Gadea, I. Paidarová, Chem. Phys. **209**, 281 (1996)
29. H. Haberland, B.v. Issendorff, R. Fröchtenicht, J.P. Toennies, J. Chem. Phys. **102**, 8773 (1995)
30. J.A. Gascón, *Electronic and Structural Properties of Rare Gas Cation Clusters*, Ph.D. dissertation, 2002, and references therein
31. H. Haberland, A. Holfmann, B.v. Issendorff, J. Chem. Phys. **103**, 3450 (1995)
32. S. Magnier, F. Oise, M. Seeuws, Mol. Phys. **89**, 711 (1996)
33. F. Borondo, R.M. Benito, in *Frontiers of Chemical Dynamics*, edited by E. Yurtsever, NATO ASI Series C **470** (Kluwer, Dordrecht, 1995); F. Borondo, R.M. Benito, in *The Physics and Chemistry of Wave Packets*, edited by J. Yeazell, T. Uzer (Wiley, New York, 2000), and references therein
34. R. Essers, J. Tennyson, P.E.S. Wormer, Chem. Phys. Lett. **89**, 223 (1982); P.V.R. Schleyer, A. Sawaryn, A.F. Reed, J. Comput. Chem. **7**, 666 (1986)
35. E. Engel, in *A Primer in Density Functional Theory*, edited by C. Fiolhais, F. Nogueira, M.A.L. Marques (Springer, Berlin, 2003)
36. M. Städele, J.A. Majewski, P. Vogl, A. Görling, Phys. Rev. Lett. **79**, 2089 (1997); T. Grabo, T. Kreibich, S. Kurth, E.K.U. Gross, in *Strong Coulomb Correlations in Electronic Structure: Beyond the Local Density Approximation*, edited by V.I. Anisimov (Gordon & Breach, Tokyo, 1998)
37. A canonical transformation to the nuclear geometrical center has been performed